THE JOURNAL OF PHYSICAL CHEMISTRY Letters

Letter

pubs.acs.org/JPCL

Evolution of Hydrogen Dynamics in Amorphous Ice with Density

A. Parmentier,[†] J. J. Shephard,[‡,§] G. Romanelli,[†] R. Senesi,[†,∥] C. G. Salzmann,*[,‡] and C. Andreani*[,†,∥]

[†]Dipartimento di Fisica and NAST Centre, Università degli Studi di Roma Tor Vergata, Via della Ricerca Scientifica 1, 00133 Roma, Italy

[‡]Department of Chemistry, University College London, 20 Gordon Street, London WC1H 0AJ, United Kingdom

[§]Department of Chemistry, Durham University, South Road, Durham DH1 3LE, United Kingdom

[∥]CNR-IPCF Sezione di Messina, Viale F. Stagno D'Alcontres 37, 98158 Messina, Italy

Supporting Information

ABSTRACT: The single-particle dynamics of hydrogen atoms in several of the amorphous ices are reported using a combination of deep inelastic neutron scattering (DINS) and inelastic neutron scattering (INS). The mean kinetic energies of the hydrogen nuclei are found to increase with increasing density, indicating the weakening of hydrogen bonds as well as a trend toward steeper and more harmonic hydrogen vibrational potential energy surfaces. DINS shows much more pronounced changes in the O−H stretching component of the mean kinetic energy going from low- to high-density amorphous ices than indicated by INS and Raman spectroscopy. This highlights the power of the DINS technique to retrieve accurate ground-state kinetic energies beyond the harmonic approximation. In a novel approach, we use information from DINS and INS to determine the anharmonicity constants of the O−H stretching modes. Furthermore, our experimental kinetic energies will serve as important benchmark values for path-integral Monte Carlo simulations.

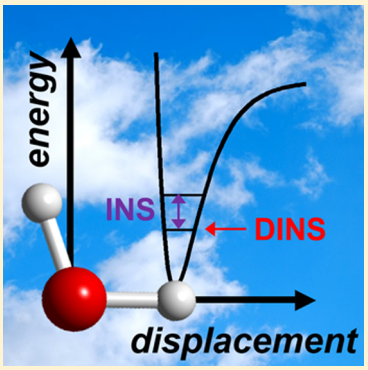

Ice is the prototype hydrogen-bonded material, and it displays immense structural complexity in terms of crystalline polymorphs and amorphous forms. At present, 16 crystalline and at least 2 families of amorphous forms of ice are known.[1−3] Using neutron diffraction, the crystal structures of the various crystalline ices have been firmly established, and the average local structures of the amorphous ices have been described.[4−6] While the approximately tetrahedral hydrogen-bonding arrangements are preserved for all amorphous forms of ice, it has been shown that low-density amorphous ice (LDA), unannealed high-density amorphous ice (uHDA), and very-high-density amorphous ice (vHDA) are structurally distinct with respect to the number of interstitial water molecules in the first coordination shell.[4,5] The average next-neighbor coordination number found at ambient pressure is four in LDA, and this number increases to five and six in uHDA and vHDA, respectively.[5] These structural differences manifest in bulk densities of 0.94 (LDA), 1.15 (uHDA), and 1.26 g cm^{-3} (vHDA) at ambient pressure and 77 K.[3,7]

The dynamics of the amorphous ices are not as well understood as their structures, and some aspects of their dynamic behavior are even highly controversial.[2,3] For example, it has been postulated that LDA undergoes a glass-to-liquid transition just before the onset of crystallization to ice I,[8] and several experimental studies have been presented in favor of this scenario;[9−13] however, it has also been argued that the true glass-to-liquid transition should be located at considerably higher temperatures and therefore be difficult to access experimentally.[14−16] A third scenario is that the step in heat capacity observed upon heating LDA is connected to the kinetic unfreezing of the reorientation dynamics of the water molecules and is therefore not due to a transition to the supercooled liquid in which translational diffusion would take place.[17,18] Similar controversial views may also apply to the low-temperature dynamics of HDA.[19−22] Furthermore, the question as to what exactly constitutes a distinct amorphous state is still debated.[3,23−25] For example, it is not clear if uHDA and vHDA are indeed distinct states or perhaps members of the same energetic megabasin.[3,25] Ultimately, definitive answers to these questions may only be found with a more detailed knowledge of the low-temperature potential energy surface of the amorphous ices.

The microscopic properties of water and ice are strongly influenced by quantum mechanical effects of their electronic structure, chemical bonding, and nuclear motion. In particular, motions involving the light hydrogen nuclei are often strongly affected by nuclear quantum effects (NQEs). Deep inelastic neutron scattering (DINS), which is performed at high momentum, $\hbar q$, and energy transfers, $\hbar\omega$, probes the quantum behavior of atomic nuclei directly through the single-particle momentum distribution, $n(p)$, and the mean kinetic energy, $\langle E_K \rangle$, which is predominantly determined by the properties of the vibrational ground state.[26] The combination of DINS with inelastic neutron scattering (INS) and Raman scattering can

Received: April 6, 2015
Accepted: May 12, 2015
Published: May 12, 2015

DOI: 10.1021/acs.jpclett.5b00711
J. Phys. Chem. Lett. 2015, 6, 2038−2042

provide additional information on the anisotropic nature of hydrogen motions in condensed systems.[27−29]

We present results on the hydrogen dynamics in LDA, uHDA, and vHDA at 80 K and ambient pressure using a combination of DINS and INS. The aim is to fully describe the properties of the hydrogen nuclei in momentum space to gain insight into their local environments and hydrogen-bond dynamics and to retrieve information about how the potential energy surfaces of the amorphous ices change as a function of density and with respect to anharmonicity.

In our DINS experiment, individual neutron Compton profiles for the hydrogen nuclei, $F_I(y,q)$, were obtained from each detector at the VESUVIO instrument at ISIS.[30−32] Figure 1a shows the angle-averaged $F_I(y,q)$ function, $\overline{F}(y,q)$, for vHDA at 80 K. Data of similar quality have been obtained for LDA and uHDA as well.

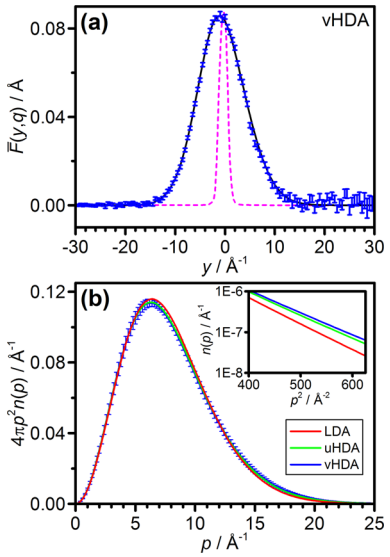

Figure 1. (a) $\overline{F}(y,q)$ of vHDA at 80 K (blue) together with best fits resulting from the averaged multivariate Gaussian model for the momentum distribution defined in eq 1 (black) and the angle-averaged instrumental resolution $\overline{R}(y,q)$ (magenta). (b) Radial momentum distribution, $4\pi p^2 n(p)$, for LDA (red), uHDA (green), and vHDA (blue). For clarity, error bars are only shown for the vHDA data. The inset shows $n(p)$ in the region where motions in the O−H stretching direction dominate.

The experimental $n(p)$ lineshapes for the amorphous ices shown in Figure 1b have been determined by modeling the momentum distributions as spherical averages of multivariate Gaussians according to[33−35]

$$4\pi p^2 n(p) = \int \frac{\delta(p - |p|)}{\sqrt{8\pi^3 \sigma_x \sigma_y \sigma_z}} \exp\left[-\frac{p_x}{2\sigma_x^2} - \frac{p_y}{2\sigma_y^2} - \frac{p_z}{2\sigma_z^2}\right] \mathrm{d}^3 p \quad (1)$$

where σ_α^2, with $\alpha = x,y,z$, represent the variance of $n(p)$ directly related to the directional mean kinetic energy along x, y, and z, $\langle E_K \rangle_\alpha$, by the expression $\langle E_K \rangle_\alpha = ((\hbar^2 \sigma_\alpha^2)/2M)$ and to the three principal frequencies, ω_α, by the expression $\sigma_\alpha^2 = ((M\omega_\alpha)/2\hbar)\coth(\beta(\hbar\omega_\alpha/2))$. (See the Supporting Information (SI) for full details.) The definitions of the x, y, and z axes, associated with a hydrogen in a H_2O molecule, are shown in Figure 2a. $\langle E_K \rangle_z$ defines the mean kinetic energy component along the O−H stretching direction, whereas the corresponding quantities in the perpendicular directions are $\langle E_K \rangle_x$ and $\langle E_K \rangle_y$, respectively. Network modes can slightly affect the principal frequencies as mentioned in the theoretical work by Lin et al., with an estimated contribution of ≤6% for polycrystalline ice.[36] The total mean kinetic energy of the hydrogen atoms, $\langle E_K \rangle$, is then obtained from the sum of the three directional components.

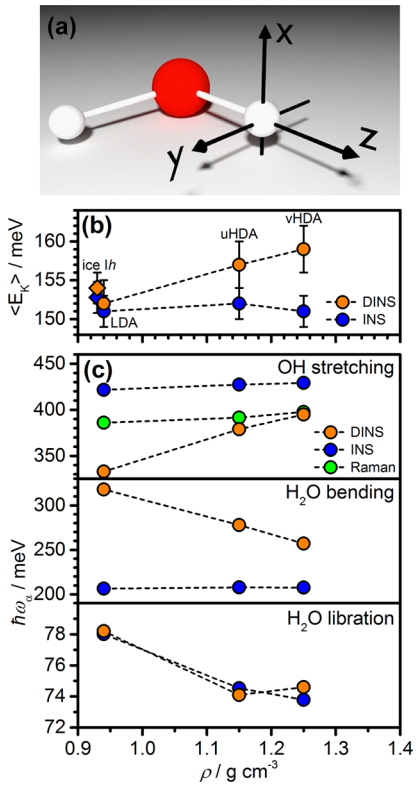

Figure 2. (a) Schematic view of the local principal axes associated with hydrogen in the water molecule. (b) $\langle E_K \rangle$ values from DINS (orange) and corresponding values obtained from INS using the harmonic model introduced by Andreani et al.[28] (blue). (c) Energies of the O−H stretching modes, $\hbar\omega_{str}$, bending modes, $\hbar\omega_{ben}$, and librational modes, $\hbar\omega_{lib}$, obtained from INS (blue) and Raman (green) as well as the corresponding values derived from DINS (orange).

Vibrations in the direction of O−H stretching (z direction) contribute primarily to the high momentum tail of the $n(p)$ momentum distribution because the hydrogen atoms are most tightly bound in this direction by the covalent O−H bond. The increased momentum width at $p > 12$ Å^{-1} with increasing density of the amorphous ice is therefore a signature of the covalent O−H bond getting stronger due to a weakening of the hydrogen-bond network (cf. insert in Figure 1b).[37]

This behavior can also be seen in Table S1 in the SI, where $\langle E_K \rangle$, $\langle E_K \rangle_\alpha$, and σ_α values are reported for LDA, uHDA, and vHDA. The difference between the $\langle E_K \rangle$ values for LDA and ice Ih[38] is small, indicating similar local environments (cf. Figure 2b). An increase in $\langle E_K \rangle$ is found with increasing density from LDA to uHDA and vHDA. $\langle E_K \rangle_z$ also increases with density from 83.3 (LDA) to 94.8 (uHDA) and 98.7 meV (vHDA), whereas for $\langle E_K \rangle_x$ and $\langle E_K \rangle_y$, the opposite trends are found. Consistent with the differences in the $n(p)$ functions, the overall increase in $\langle E_K \rangle$ with density is therefore mainly caused by the contributions from $\langle E_K \rangle_z$.

In addition to the DINS information on the ground state the transition from the ground state to the first excited states is

DOI: 10.1021/acs.jpclett.5b00711
J. Phys. Chem. Lett. 2015, 6, 2038−2042

provided by INS and Raman spectroscopy. While INS reflects the hydrogen-projected density of vibrational states, Raman intensity is associated with a change in polarizability of a specific vibration. For ice, in particular, this means that the in-phase coupled symmetric stretching vibration of H_2O is the strongest intensity contribution to the Raman spectrum in the O−H region.[39] The INS spectra in Figure 3a show the energy

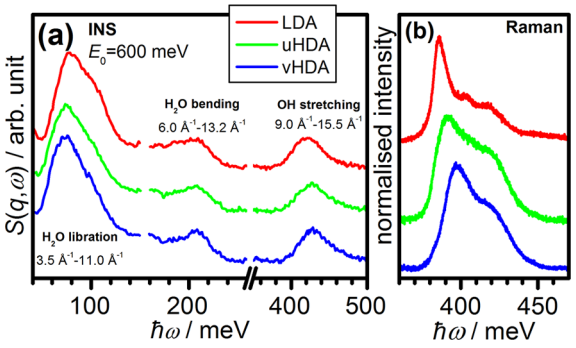

Figure 3. (a) Experimental dynamic structure factor $S(q,\omega)$ of LDA (red), uHDA (green), and vHDA (blue) at 80 K. The spectra were obtained after averaging over the indicated q ranges (cf. Figure S2 in the SI). (b) Raman spectra of the same samples in the coupled ν(O−H) stretching region.

transfer, $\hbar\omega$, of the main inter- and intramolecular bands: librations or hindered rotations of water molecules at ∼80 meV, H−O−H bending at ∼210 meV, and O−H stretching at ∼420 meV. Figure 3b shows the intensity-normalized Raman spectra in the O−H stretching region. The lower frequencies of the main feature in the Raman spectra compared with the corresponding INS spectra are consistent with the lower frequency of the symmetric stretching mode for water in the gas phase compared with the antisymmetric mode.[40,41]

The peak positions of stretching, bending, and libration modes from INS and Raman spectra of the amorphous ices are summarized in Figure 2c. The notable trends are the blue shifts of the O−H stretching bands and the red shift of the libration band going from LDA to uHDA and vHDA.

The blue shifts in the O−H stretching peak positions with increasing density indicate stronger covalent O−H bonds due to weakening of the hydrogen bonds. This is fully consistent with trends of the stretching modes observed for the crystalline phases of ice at liquid nitrogen temperature and ambient pressure[42] as well as for water and supercooled water.[29] For example, the symmetric stretching feature in the Raman spectra increases from 381.9 meV in ice I*h* (0.93 g cm^{-3}) to 416.5 meV in ice VIII (1.483 g cm^{-3}), the densest phase of ice that can be recovered at ambient pressure.[43] These spectroscopic changes can be rationalized by an increase in coordination number from four water molecules in ice I*h* (all hydrogen bonded) to eight in ice VIII (four hydrogen bonded, four interstitial molecules). The interstitial molecules cause a lengthening and weakening of the hydrogen bonds. These phenomena are typical examples of the pressure−coordination rule and the consequent pressure−distance paradox.[44,45] The weakening of the hydrogen-bonded network as density increases consequently leads to a red shift of the librational modes that are caused by the hindered rotations of rigid water molecules against their local hydrogen bond network.

The trends in the DINS, INS, and Raman data paint a consistent *qualitative* picture of the local hydrogen dynamics of the amorphous ices, whereby the hydrogen atoms are more constrained/localized in the lower density forms due to the stronger hydrogen-bond network.

Yet *quantitatively* speaking, much greater changes with density are observed in $\hbar\omega_{str}$ derived from DINS compared with the corresponding INS values (cf. Figure 2c). As previously discussed, stretching vibrations represent the most significant contributions to $\langle E_K \rangle$ and consequently the increase in the DINS $\langle E_K \rangle$ values as a function of density originates from the $\langle E_K \rangle_z$. Unlike in INS, the strengthening of covalent bond in the ground states is fully captured in the DINS analysis, as highlighted in the wings of the $n(p)$ lineshapes (cf. Figure 1b, inset) and by the differences between $\langle E_K \rangle$ and $\langle E_K \rangle_z$ of the amorphous ices (cf. Figure 2b,c). We stress that the harmonic-decoupled model used to relate the $\langle E_K \rangle_\alpha$ to the stretching, bending, and libration energies is carried out within an isolated-molecule framework, and it provides a qualitative insight into the influence of the connected hydrogen-bond network on the single-particle properties probed here. The lower values of $\langle E_K \rangle$ and $\langle E_K \rangle_z$ in LDA compared with uHDA and vHDA also indicate a more anharmonic and shallower hydrogen potential-energy surface. These values directly reflect changes in anharmonicity of the hydrogen potential surface as the density increases and the hydrogen bonds weaken, and the change is most evident along the z direction, which captures mostly the shape of the effective hydrogen nucleus potential along the O−H bond direction.

The increase in the $\langle E_K \rangle$ values derived from DINS with density is in contrast with recent path-integral molecular dynamics simulations of high-density amorphous ice,[46] where the $\langle E_K \rangle$ value of the ground state calculated for HDA was ∼2 meV lower than in ice I*h*. The authors interpreted this finding as due to larger quantum delocalization of the hydrogen atoms in HDA compared with ice I*h* at the same temperature. Our results are instead consistent with stronger covalent O−H bonds in uHDA and vHDA compared with ice I*h*, in *qualitative* agreement with previous INS studies.[47] Also, a computational study on ice VII has shown that $\langle E_K \rangle$ decreases as the covalent O−H bonds weaken upon compression.[48]

The three $\langle E_K \rangle_\alpha$ values derived from INS shown in Table S1 in the SI for the amorphous ices and ice I*h* are obtained within the harmonic model and with the assumption of decoupling of both inter and intramolecular modes (see SI for further details).[28] Within this framework, this suggests that the local hydrogen dynamics in terms of both $\langle E_K \rangle$ and $\langle E_K \rangle_\alpha$ components have little density/structure dependence. As far as the librations are concerned, Figure 2c shows very similar frequency values from INS and DINS, indicating a small degree of anharmonicity of the libration modes. For the bending modes, INS allows a direct measurement of the bending energy; however, the coupling of internal modes affects the DINS-derived bending energy, and this is likely to be responsible for the observed differences between the INS and DINS energies. The behavior of the bending energy from DINS is consistent with changes of coupling of internal modes as the surrounding network evolves from LDA to vHDA.

In a final step, we present a new way of quantifying the degree of anharmonicity of the O−H stretching modes by a combined use of DINS and INS data. The absolute energy of the first vibrationally excited state can be calculated as the sum of the ground-state energy from DINS plus the experimental excitation energy from INS. As shown in eq 2, this then equals the energy of the first excited state calculated using a harmonic

DOI: 10.1021/acs.jpclett.5b00711
J. Phys. Chem. Lett. 2015, 6, 2038−2042

model, which is corrected by a term containing the anharmonicity constant, χ_e.[49]

$$\frac{\hbar\omega_{str}^{DINS}}{2} + \hbar\omega_{str}^{INS} = \frac{3}{2}\hbar\omega_{str}^{INS}\left(1 - \frac{3}{2}\chi_e\right) \quad (2)$$

Using this approach, χ_e values of 0.046 (LDA), 0.025 (uHDA), and 0.018 (vHDA) are obtained, which now provide a quantitative measure for the much more pronounced anharmonicity of the O−H stretching modes in LDA compared with the HDAs.

In summary, experimental DINS results of the amorphous ices as a function of density are reported and compared with the hydrogen excitation energies for inter- and intramolecular vibrations obtained using INS and Raman spectroscopy. The capability of DINS to directly probe the total and directional mean kinetic energies of ground-state motions has allowed the pronounced softening of the effective stretching potential in LDA compared with the HDAs to be revealed. As the hydrogen bonding weakens with increasing density, the curvature of the effective potential increases and its shape becomes similar to the shapes inferred from INS within the harmonic assumption. Hydrogen bonding can therefore be viewed as the main cause for anharmonicity in amorphous ice.

It was recently shown that theories using harmonic or quasi-harmonic descriptions of quantum effects related to zero-point vibrations lead to overestimation of the atomic and molecular kinetic energies that are greater than those obtained from path integral molecular dynamics simulations.[36,50] The shortcomings of the harmonic description originate from the stiffer underlying effective potentials than those derived from ab initio methods. Here we provided direct experimental evidence of the relevance of anharmonic effects in the quantum dynamics of the hydrogen nuclei in the amorphous ices and their evolution with increasing density. Most significantly, the DINS experiments allowed us to directly probe the increase in the kinetic energy along the O−H bond direction as the curvature of the effective potential increases and becomes more harmonic with increasing density. The subtlety of such anharmonic contributions has been derived by combining and comparing techniques sensitive to the single-particle hydrogen wave function such as DINS and techniques sensitive to vibrational energy differences such as INS and Raman.

EXPERIMENTAL METHODS

The amorphous H_2O ices samples were prepared using a piston cylinder setup as described in ref 17 and the SI. The DINS measurements were performed using the VESUVIO instrument at the ISIS spallation neutron and muon source (Rutherford Appleton Laboratory, U.K.),[30−32] which uses incident energies in the range of 1−800 eV. The INS data were recorded using the MARI instrument also at ISIS, and a Renishaw Ramascope spectrometer (632.8 nm) was used to obtain Raman spectra.

ASSOCIATED CONTENT

Supporting Information

Details of sample preparation; experimental procedures for DINS, INS, and Raman measurements; and DINS data reduction and analysis. The Supporting Information is available free of charge on the ACS Publications website at DOI: 10.1021/acs.jpclett.5b00711.

AUTHOR INFORMATION

Corresponding Authors

*E-mail: c.salzmann@ucl.ac.uk (C.G.S.).
*E-mail: carla.andreani@uniroma2.it (C.A.).

Notes

The authors declare no competing financial interest.

ACKNOWLEDGMENTS

We thank the Royal Society (C.G.S., UF100144), the EPSRC (J.J.S.), and the Leverhulme Trust (RPG-2014-04) for financial support. This work was partially supported within the CNR-STFC Agreement (2014-2020) concerning collaboration in scientific research at the spallation neutron source ISIS. We are grateful to ISIS for access to the VESUVIO and MARI instruments.

REFERENCES

(1) Falenty, A.; Hansen, T. C.; Kuhs, W. F. Formation and Properties of Ice XVI Obtained by Emptying a Type sII Clathrate Hydrate. *Nature* **2014**, *516*, 231−233.
(2) Salzmann, C. G.; Radaelli, P. G.; Slater, B.; Finney, J. L. The Polymorphism of Ice: Five Unresolved Questions. *Phys. Chem. Chem. Phys.* **2011**, *13*, 18468−18480.
(3) Loerting, T.; Winkel, K.; Seidl, M.; Bauer, M.; Mitterdorfer, C.; Handle, P. H.; Salzmann, C. G.; Mayer, E.; Finney, J. L.; Bowron, D. T. How Many Amorphous Ices Are There? *Phys. Chem. Chem. Phys.* **2011**, *13*, 8783−8794.
(4) Finney, J. L.; Bowron, D. T.; Soper, A. K.; Loerting, T.; Mayer, E.; Hallbrucker, A. Structure of a New Dense Amorphous Ice. *Phys. Rev. Lett.* **2002**, *89*, 205503−1.
(5) Finney, J. L.; Hallbrucker, A.; Kohl, I.; Soper, A. K.; Bowron, D. T. Structures of High and Low Density Amorphous Ice by Neutron Diffraction. *Phys. Rev. Lett.* **2002**, *88*, 22503−1.
(6) Bowron, D. T.; Finney, J. L.; Hallbrucker, A.; Kohl, I.; Loerting, T.; Soper, A. K. The Local and Intermediate Range Structures of the Five Amorphous Ices at 80 K and Ambient Pressure: A Faber-Ziman and Bhatia-Thornton analysis. *J. Chem. Phys.* **2006**, *125*, 194502.
(7) Loerting, T.; Salzmann, C.; Kohl, I.; Mayer, E.; Hallbrucker, A. A Second Distinct Structural "State" of High-density Amorphous Ice at 77 K and 1 bar. *Phys. Chem. Chem. Phys.* **2001**, *3*, 5355−5357.
(8) Johari, G. P.; Hallbrucker, A.; Mayer, E. The Glass-liquid Transition of Hyperquenched Water. *Nature* **1987**, *330*, 552−553.
(9) Johari, G. P. Liquid State of Low-Density Pressure-Amorphized Ice above Its T_g. *J. Phys. Chem. B* **1998**, *102*, 4711−4714.
(10) Smith, R. S.; Kay, B. D. The Existence of Supercooled Liquid Water at 150 K. *Nature* **1999**, *398*, 788−791.
(11) Seidl, M.; Elsaesser, M. S.; Winkel, K.; Zifferer, G.; Mayer, E.; Loerting, T. Volumetric Study Consistent with a Glass-to-liquid Transition in Amorphous Ices under Pressure. *Phys. Rev. B* **2011**, *83*, 100201.
(12) Amann-Winkel, K.; Löw, F.; Handle, P. H.; Knoll, W.; Peters, J.; Geil, B.; Fujara, F.; T, L. Limits of Metastability in Amorphous Ices: The Neutron Scattering Debye-Waller Factor. *Phys. Chem. Chem. Phys.* **2013**, *14*, 16386−16391.
(13) Löw, F.; Amann-Winkel, K.; Loerting, T.; Fujara, F.; Geil, B. Ultra-slow Dynamics in Low Density Amorphous Ice Revealed by Deuteron NMR: Indication of a Glass Transition. *Phys. Chem. Chem. Phys.* **2013**, *15*, 9308−9314.
(14) Velikov, V.; Borick, S.; Angell, C. A. The Glass Transition of Water, Based on Hyperquenching Experiments. *Science* **2001**, *294*, 2335−2338.
(15) Yue, Y.; Angell, C. A. Clarifying The Glass-transition Behaviour of Water by Comparison with Hyperquenched Inorganic Glasses. *Nature* **2004**, *427*, 717−720.
(16) Angell, C. A. Insights into Phases of Liquid Water from Study of Its Unusual Glass-forming Properties. *Science* **2008**, *319*, 582−587.

DOI: 10.1021/acs.jpclett.5b00711
J. Phys. Chem. Lett. 2015, 6, 2038−2042

(17) Shephard, J. J.; Evans, J. S. O.; Salzmann, C. G. Structural Relaxation of Low-Density Amorphous Ice upon Thermal Annealing. *J. Phys. Chem. Lett.* **2013**, *4*, 3672−3676.
(18) Fisher, M.; Devlin, J. P. Defect Activity in Amorphous Ice from Isotopic Exchange Data: Insight into the Glass Transition. *J. Phys. Chem.* **1995**, *99*, 11584.
(19) Mishima, O. The Glass-to-liquid Transition of the Emulsified High-density Amorphous Ice Made by Pressure-induced Amorphization. *J. Chem. Phys.* **2004**, *121*, 3161−3164.
(20) Andersson, O. Glass−liquid Transition of Water at High Pressure. *Proc. Natl. Acad. Sci. U.S.A.* **2011**, *108*, 11013−11016.
(21) Handle, P. H.; Seidl, M.; T, L. Relaxation Time of High-Density Amorphous Ice. *Phys. Rev. Lett.* **2012**, *108*, 225901.
(22) Amann-Winkel, K.; Gainaru, K.; Handle, P. H.; Seidl, M.; Nelson, H.; Böhmer, R.; Loerting, T. Water's Second Glass Transition. *Proc. Natl. Acad. Sci. U.S.A.* **2013**, *110*, 17720−17725.
(23) Klotz, S.; Hamel, G.; Loveday, J. S.; Nelmes, R. J.; Guthrie, M. Structure of High-Density Amorphous Ice under Pressure. *Phys. Rev. Lett.* **2002**, *89*, 285502−1.
(24) Tulk, C. A.; Benmore, C. J.; Urquidi, J.; Klug, D. D.; Neuefeind, J.; Tomberli, B.; Egelstaff, P. A. Structural Studies of Several Distinct Metastable Forms of Amorphous Ice. *Science* **2002**, *297*, 1320−1323.
(25) Salzmann, C. G.; Loerting, T.; Klotz, S.; Mirwald, P. W.; Hallbrucker, A.; Mayer, E. Isobaric Annealing of High-density Amorphous Ice between 0.3 and 1.9 GPa: In Situ Density Values and Structural Changes. *Phys. Chem. Chem. Phys.* **2006**, *8*, 386−397.
(26) Andreani, C.; Colognesi, D.; Mayers, J.; Reiter, G.; Senesi, R. Measurement of Momentum Distribution of Light Atoms and Molecules in Condensed Matter Systems using Inelastic Neutron Scattering. *Adv. Phys.* **2005**, *54*, 377−469.
(27) Finkelstein, Y.; Moreh, R. Temperature Dependence of the Proton Kinetic Energy in Water Between 5 and 673 K. *Chem. Phys.* **2014**, *431*, 58−63.
(28) Andreani, C.; Romanelli, G.; Senesi, R. A Combined INS and DINS Study of Proton Quantum Dynamics of Ice and Water Across the Triple Point and in the Supercritical Phase. *Chem. Phys.* **2013**, *427*, 106−110.
(29) Senesi, R.; Flammini, D.; Kolesnikov, A. I.; Murray, E. D.; Galli, G.; Andreani, C. The Quantum Nature of the OH Stretching Mode in Ice and Water Probed by Neutron Scattering Experiments. *J. Chem. Phys.* **2013**, *139*, 074504.
(30) Mayers, J.; Reiter, G. The VESUVIO Electron Volt Neutron Spectrometer. *Meas. Sci. Technol.* **2012**, *23*, 045902.
(31) Senesi, R.; Andreani, C.; Bowden, Z.; Colognesi, D.; Degiorgi, E.; Fielding, A. L.; Mayers, J.; Nardone, M.; Norris, J.; Praitano, M.; et al. VESUVIO: A Novel Instrument for Performing Spectroscopic Studies in Condensed Matter with eV Neutrons at the ISIS Facility. *Physica B* **2012**, *276−78*, 200−201.
(32) Schooneveld, E. M.; Mayers, J.; Rhodes, N. J.; Pietropaolo, A.; Andreani, C.; Senesi, R.; Gorini, G.; Perelli-Cippo, E.; Tardocchi, M. Foil Cycling Technique for the VESUVIO Spectrometer Operating in the Resonance Detector Configuration. *Rev. Sci. Instrum.* **2006**, *77*, 095103.
(33) Romanelli, G.; Ceriotti, M.; Manolopoulos, D. E.; Pantalei, C.; Senesi, R.; Andreani, C. Direct Measurement of Competing Quantum Effects on the Kinetic Energy of Heavy Water upon Melting. *J. Phys. Chem. Lett.* **2013**, *4*, 3251−3256.
(34) Andreani, C.; Degiorgi, E.; Senesi, R.; Cilloco, F.; Colognesi, D.; Mayers, J.; Nardone, M.; Pace, E. Single Particle Dynamics in Fluid and Solid Hydrogen Sulphide: An Inelastic Neutron Scattering Study. *J. Chem. Phys.* **2001**, *114*, 387−398.
(35) Flammini, D.; Pietropaolo, A.; Senesi, R.; Andreani, C.; McBride, F.; Hodgson, A.; Adams, M. A.; Lin, L.; Car, R. Spherical Momentum Distribution of the Protons in Hexagonal Ice from Modeling of Inelastic Neutron Scattering Data. *J. Chem. Phys.* **2012**, *136*, 024504.
(36) Lin, L.; Morrone, J. A.; Car, R.; Parrinello, M. Momentum Distribution, Vibrational Dynamics, and the Potential of Mean Force in Ice. *Phys. Rev. B* **2011**, *83*, 220302.
(37) Pantalei, C.; Pietropaolo, A.; Senesi, R.; Imberti, S.; Andreani, C.; Mayers, J.; Burnham, C.; Reiter, G. Proton Momentum Distribution of Liquid Water from Room Temperature to the Supercritical Phase. *Phys. Rev. Lett.* **2008**, *100*, 177801/1−4.
(38) Senesi, R.; Romanelli, G.; Adams, M. A.; Andreani, C. Temperature Dependence of the Zero Point Kinetic Energy in Ice and Water Above Room Temperature. *Chem. Phys.* **2013**, *427*, 111−116.
(39) Whalley, E. A Detailed Assignment of the O-H Stretching Bands of Ice I. *Can. J. Chem.* **1977**, *55*, 3429−3441.
(40) Bernath, P. F. The Spectroscopy of Water Vapour: Experiment, Theory and Applications. *Phys. Chem. Chem. Phys.* **2002**, *4*, 1501−1509.
(41) Tennyson, J.; Bernath, P. F.; Brown, L. R.; Campargue, A.; Császár, A. G.; Daumont, L.; Gamache, R. R.; Hodges, J. T.; Naumenko, O. V.; Polyansky, O. L.; et al. A Database of Water Transitions from Experiment and Theory (IUPAC Technical Report). *Pure Appl. Chem.* **2014**, *86*, 71−83.
(42) Minceva-Sukarova, B.; Sherman, W. F.; Wilkinson, G. R. The Raman spectra of Ice (I_h, II, III, V, VI and IX) as Functions of Pressure and Temperature. *J. Phys. C* **1984**, *17*, 5833−5850.
(43) Klotz, S.; Strässle, T.; Salzmann, C. G.; Philippe, J.; Parker, S. F. Incoherent Inelastic Neutron Scattering Measurements on Ice VII: Are There Two Kinds of Hydrogen Bonds in Ice? *Europhys. Lett.* **2005**, *72*, 576−582.
(44) Müller, U. *Anorganische Strukturchemie*; Teubner Studienbücher: Stuttgart, Germany, 1996.
(45) Prewitt, C. T.; Downs, R. T. High-Pressure Crystal Chemistry. *Rev. Mineral.* **1998**, *37*, 283−317.
(46) Herrero, C. P.; Ramirez, R. High-Density Amorphous Ice: A Path-Integral Simulation. *J. Chem. Phys.* **2012**, *137*, 104505/1−11.
(47) Kolesnikov, A. I.; Li, J.; Parker, S. F.; Eccleston, R. S.; Loong, C.-K. Vibrational Dynamics of Amorphous Ice. *Phys. Rev. B* **1999**, *59*, 3569−3578.
(48) Finkelstein, Y.; Moreh, R. Proton Dynamics in Ice VII at High Pressures. *J. Chem. Phys.* **2013**, *139*, 044716.
(49) Wilson, E. B.; Decius, J. C.; Cross, P. C. *Molecular Vibrations: The Theory of Infrared and Raman Vibrational Spectra*; Dover Publications: New York, 2003.
(50) Ramirez, R.; Neuerburg, N.; Fernandez-Serra, M. V.; Herrero, C. P. Quasi-harmonic Approximation of Thermodynamic Properties of Ice Ih, II, and III. *J. Chem. Phys.* **2012**, *137*, 044502.

DOI: 10.1021/acs.jpclett.5b00711
J. Phys. Chem. Lett. 2015, 6, 2038−2042